Low temperature fabrication of hydrangea-like $NiCo_2S_4$ as electrode materials for high performance supercapacitors

Fenglin Zhao [a], Wanxia Huang [a,*], Qiwu Shi [a,*], Dengmei Zhou [a], Ling Zhao [a], Hongtao Zhang [b]

[a] College of Materials Science and Engineering, Sichuan University, Chengdu 610065, China

[b] Department of Materials, Loughborough University, Leicester LE11 3TU, UK

[*] Corresponding authors. E-mail: huangwanxia@scu.edu.cn; shiqiwu_cd@126.com

Abstract

Hydrangea-like $NiCo_2S_4$ as electrode materials for high performance supercapacitors was synthesized by using a facile low temperature (90 °C) two-step hydrothermal technique without surfactant or template. The special hydrangea-like structure and large specific surface area (74.8 m^2/g) provided plenty of electro active sites which were beneficial to superior pseudocapacitive performance of $NiCo_2S_4$. The supercapacitors performance of $NiCo_2S_4$ was investigated by a three-electrode system. $NiCo_2S_4$ exhibited high specific capacitance with 1475 F g^{-1} at a current density of 3 A g^{-1}, and a fairly high rate capacity with 1152 F g^{-1} at 20 A g^{-1}. These results indicate that low temperature hydrothermal is a very promising method to prepare electrode materials for supercapacitors.

Key words: $NiCo_2S_4$; Low temperature; Hydrothermal technique; Electrical properties; Energy storage and conversion

1. Introduction

Recently, supercapacitors hold considerable promise in energy storage and conversion systems due to their advantages of short charge/discharge time, long cycling lifetime and ultrahigh power density [1-3]. The electrochemical performances of supercapacitors mainly depend on the property of electrode materials, including carbon materials, conducting polymers and transition metal oxides/hydroxides/sulfides [4]; Among them, transition metal oxides/sulfides (such as MoS_2 [5], CuS [6], Ni_3S_2 [7]) are the most promising candidate materials for supercapacitors. Compared with binary metal oxides/sulfides, ternary metal oxides/sulfides exhibit much higher specific capacitance owing to the rich redox reaction sites of their mixed valence and the synergistic effect of different cations [8]. Very recently, $NiCo_2S_4$ attracts much interest since its electrical conductivity is nearly 100 times higher than that of $NiCo_2O_4$, which has a significant impact on its excellent electrochemistry performance [9] and [10].

In general, the hydrothermal synthesis of $NiCo_2S_4$ by method is conducted at relatively high temperature from 140 °C to 200 °C [11-13]. Nevertheless, the energy efficiency, security and reliability are compromised by the high temperature. Hence, it is necessary to explore a lower temperature, scalable processing of $NiCo_2S_4$. In the present paper,

hydrangea-like $NiCo_2S_4$ as supercapacitors electrode materials with high performance was successfully synthesized by low temperature (90 °C) hydrothermal technique.

2 Experimental

2.1. Materials synthesis

1.164g $Co(NO_3)_2 \cdot 6H_2O$, 0.582g $Ni(NO_3)_2 \cdot 6H_2O$ and 0.616g hexamethylenetetramine were dissolved into 60 mL deionized water/ethanol solvent (2:1 by volume) and stirred for 20 min. The mixed solution was transferred to a Teflon-lined stainless steel autoclave (TSSA) and heated in an oven at 90 °C for 48 h. Then the products were washed several times with deionized water and ethanol by centrifugation, and dried in a vacuum oven at 70 °C for 10 h to obtain the NiCo-precursor. Then, 0.5g $Na_2S \cdot 9H_2O$ was added into 70 mL deionized water under stirring for 20 min and the NiCo-precursor was added into above solution with continuous stirring for another 30 min. The mixed solution was again transferred into the TSSA and heated to 90 °C for 48 h. After the same washing and drying steps as described above, $NiCo_2S_4$ was attained.

2.2. Materials characterization

The crystalline structure and chemical composition of the samples were examined by X-ray diffraction (XRD, Rigaku D/max-2200), X-ray photoelectron spectroscopy (XPS, Thermo Scientific, ESCALAB 250xi), respectively. The micro-morphology was characterized by scanning electron microscopy (SEM, Hitachi S-4800) and high resolution transmission electron microscopy (HRTEM, FEI Tecnai G20). The Brunauer-Emmett-Teller (BET, Quadrasorb evo) specific surface area of the sample was measured by N_2 adsorption-desorption.

The electrochemical properties of $NiCo_2S_4$ were evaluated by three-electrode system by CHI660E electrochemical workstation. The working electrode was prepared by mixing 80 wt% $NiCo_2S_4$, 10 wt% acetylene black and 10 wt% PVDF. Platinum foil and Ag/AgCl were used as counter and reference electrode, respectively. The loading mass on Ni foam is about 4 mg and 3 M KOH was used as aqueous electrolyte.

3. Results and discussion

The phase of the product was investigated by XRD and the corresponding result is showed in Fig. 1. The diffraction peaks at 26.6°, 31.5°, 38.4°, 50.4° and 55.4° can all be well indexed to the (220), (311), (400), (511) and (440) planes of a cubic $NiCo_2S_4$ (JCPDF 20–0782) phase, respectively. The XPS analysis (Fig. S1) indicates the Ni 2p spectrum was fitted with two spin-orbit doublets (Ni^{2+} and Ni^{3+}) and two shake-up satellites (“Sat”). The same as Co 2p spectrum. As for the S 2p spectrum, the peaks at 161.5 eV and 162.6 eV correspond to the S $2p_{3/2}$ and S $2p_{1/2}$, respectively. These XPS

results indicate the samples contain Ni^{2+}, Ni^{3+}, Co^{2+}, Co^{3+} and S^{2-}, which match well with the results of $NiCo_2S_4$ in literature [9,11].

Fig. 2 shows the morphology and microstructure features of the $NiCo_2S_4$. As shown in Fig. 2a and b, $NiCo_2S_4$ shows special three-dimensional (3D) hydrangea-like structure with many interconnected nanosheets. Moreover, higher magnification SEM image (Fig. S2) displays that the surface of the nanosheets contains plenty of depressions, which can greatly increase the electrochemically active sites. TEM image (Fig. 2c) shows the porous, ultrathin characteristics of the nanosheets and the thickness is about 10–20 nm. The HRTEM image (Fig. 2d) displays a clear lattice fringe and the measured lattice fringe spacing is 0.28 nm corresponding to (311) plane of $NiCo_2S_4$.

The N_2 adsorption-desorption isotherm and pore size distribution of $NiCo_2S_4$ were investigated and shown in Fig. 3. The adsorption-desorption plots belong to type IV [14,15] isotherm and a hysteresis loop with a window of 0.4–1 P/P_0 is observed which suggests the porous structure of the as-prepared $NiCo_2S_4$. The pore size distribution was calculated by Barrett−Joyner−Halenda method and the graph (Fig. 3b) exhibits sharp size distribution ranging from 1 to 4 nm and the pore radius centered at 1.9 nm, which is ideal size for ion transports. Besides, the BET surface area can be calculated to be 74.8 m^2/g, which is larger than most of the reported results (42.79 $m^2\ g^{-1}$, 37.8 $m^2\ g^{-1}$) [4, 12].

Fig. 4a shows the cyclic voltammetry (CV) curves of $NiCo_2S_4$ at scanning rate of 2, 5, 10 mV s^{-1} in a voltage window of −0.1 to 0.5 V. A pair of redox peaks can be clearly observed which demonstrate the typical pseudocapacitive behavior of $NiCo_2S_4$. It can be attributed to Faradaic reversible redox reactions of $Ni^{2+}/Ni^{3+}$and $Co^{2+}/Co^{3+}/Co^{4+}$ transition to NiSOH, CoSO, CoSOH [11] and [12]. With the increasing scan rate, the anodic peaks shift towards higher potential and the cathodic peaks shift towards lower potential which is induced by greater electric polarization [7].

The charge storage capacity of electrode materials was investigated by galvanostatic charge/discharge (GCD). The GCD curves of $NiCo_2S_4$ with a potential window of −0.1 to 0.4 V at different current densities are shown in Fig. 4b. It can be observed that the GCD curves are nearly symmetric which implies excellent coulombic efficiency. In addition, the nonlinear GCD curves demonstrate their typical Faradic reactions which are in good agreement with the CV curves. The specific capacitance C_m (F g^{-1}) can be calculated from the following formula [10]:

$$C_m = \frac{I\Delta t}{m\Delta V} \quad (1)$$

Where I is the applied discharge current (A), Δt is the discharge time (s), m is the mass of the active material (g), ΔV is the potential drop during discharge (V). Thus, the

specific capacitance of $NiCo_2S_4$ can be calculated to be 1475, 1420, 1356, 1332, 1243 and 1152 F g^{-1} at the current density of 3, 5, 8, 10, 15 and 20 A g^{-1}, respectively; and the results are higher than most of the reported in literature [4,12,13] Clearly, the electrode displays an excellent capacity retention rate of 78.1% at 20 A g^{-1} (compared with 3 A g^{-1}) which shows the potential in high rate application.

To further explore the reason of the excellent $NiCo_2S_4$ electrochemical property, EIS measurements were carried out by applying an AC voltage at a frequency ranging from 10^{-2} Hz to 10^5 Hz. As shown in Fig. 4d, the Nyquist plots consist of a quasi-semicircle at high frequency region and a more than 70° sloped line at low frequency region, which implies its typical capacitor behavior. The EIS analysis indicates charge transfer resistance is 0.13 Ω and internal resistance is 0.97 Ω, which indicate the electronic conductivity of the as-prepared $NiCo_2S_4$ is excellent.

The superior pseudocapacitive performance of $NiCo_2S_4$ can be attributed to the following factors. Firstly, the synergistic effect between the nickel/cobalt ions leads to high specific capacitance [16]. Secondly, the low resistance of $NiCo_2S_4$ is favorable to fast electron transfer and enhance charge-discharge rate performance. Thirdly, the special 3D hydrangea-like structure provide more electro active sites for Faradic reactions and it shorten the distance of electrolyte/electrode materials, which is beneficial for the rapid transportation of ions and electrons at high rate.

4. Conclusions

Hydrangea-like $NiCo_2S_4$ were synthesized by low temperature (90 °C) hydrothermal method. Owing to the favorable 3D hydrangea-like structure, high specific surface area and high electronic conductivity, the as-prepared $NiCo_2S_4$ electrode exhibited excellent pseudocapacitive performances. It delivered high specific capacitance of 1475 F g^{-1} (3 A g^{-1}) and capacity retention rate of 78.1% at 20 A g^{-1}. These findings suggest that the low temperature hydrothermal method may provide an alternative processing route to fabricate $NiCo_2S_4$ electrode materials.

Acknowledgments

The authors would like to thank the financial support from National Natural Science Foundation of China (No. 61271075); Linzhu Yu for help with SEM and Yong Jin for help with XRD.

References

[1] P. Simon, Y. Gogotsi, Nature Materials 7 (2008) 845-854.

[2] A. González, E. Goikolea, J. A. Barrena, R. Mysyk, Renewable and Sustainable Energy Reviews 58 (2016) 1189-1206.

[3] X. Liu, J. Zhang, K. Huang, P. Hao, Chemical Engineering Journal 302 (2016) 437-445.
[4] Y. Zhu. , Z. Wu, M. Jing, X. Yang, W. Song, X Ji, Journal of Power Sources 273 (2015) 584-590.
[5] K. Huang, L. Wang, J. Zhang, L. Wang, Y. Mo, Energy 67 (2014) 234-240.
[6] K. Huang, J. Zhang, K. Xing, Electrochimica Acta 149 (2014) 28-33.
[7] Z. Zhang, Z. Huang, L. Ren, Y. Shen, X. Qi, J. Zhong, Electrochimica Acta 149 (2014) 316-323.
[8] X. Rui, H. Tan, Q. Yan, Nanoscale 6(2014) 9889-9924.
[9] H. Chen, J. Jiang, L. Zhang, H. Wan, T. Qi, D. Xia, Nanoscale 5 (2013) 8879-8883.
[10] C. Xia, P. Li, A. N. Gandi, U. Schwingenschlogl, H. N. Alshareef, Chem. Mater. 27(2015) 6482-6485.
[11] X. Xiong, G. Waller, D. Ding, D. Chen, B. Rainwater, B. Zhao, et al., Nano Energy 16 (2015) 71-80.
[12] Z. Wu, X. Pu, X. Ji, Y. Zhu, M. Jing, Q. Chen, et al., Electrochimica Acta 174 (2015) 238-245.
[13] Y. Xiao, D. Su, X. Wang, L. Zhou, S. Wu, F. Li, et al., Electrochimica Acta 176 (2015) 44-50.
[14] J Li, W Zhang, G Zan, Q Wu, Dalton Transactions 45(2016) 12790-12799.
[15] J Li, G Zan, Q Wu, Journal of Materials Chemistry A 4(2016) 9097-9105.
[16] Y. Tang, T. Chen, S. Yu, Y. Qiao, S. Mu, S. Zhang, et al., W. Huang, F. Gao, Journal of Power Sources 295 (2015) 314-322.

Figure captions

Fig. 1 XRD pattern of $NiCo_2S_4$.

Fig. 2 SEM (a, b), TEM(c) and HRTEM (d) images of $NiCo_2S_4$.

Fig. 3 Nitrogen adsorption-desorption isotherm and BJH pore size distribution of $NiCo_2S_4$.

Fig. 4 (a) CV curves of the $NiCo_2S_4$ electrode at various scan rates; (b) GCD curves of the $NiCo_2S_4$ electrodes at various current densities; (c) The specific capacitance change of the $NiCo_2S_4$ electrode at different current densities; (d) Nyquist plots impedance of $NiCo_2S_4$ electrode.

Fig. S1 XPS pattern of $NiCo_2S_4$; (a)Ni, (b) Co and (c)S.

Fig. S2 High-magnification SEM images of $NiCo_2S_4$

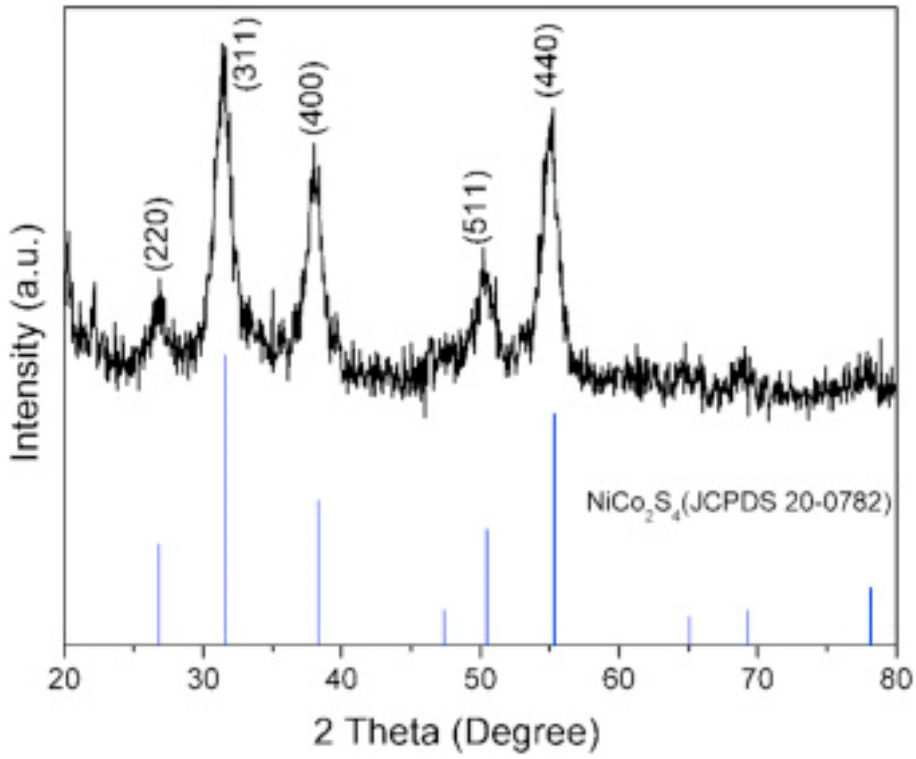
(220)
(311)
(400)
(511)
(440)
Intensity (a.u.)
NiCo2S4(JCPDS 20-0782)
20
30
40
50
60
70
80
2 Theta (Degree)

Fig. 1

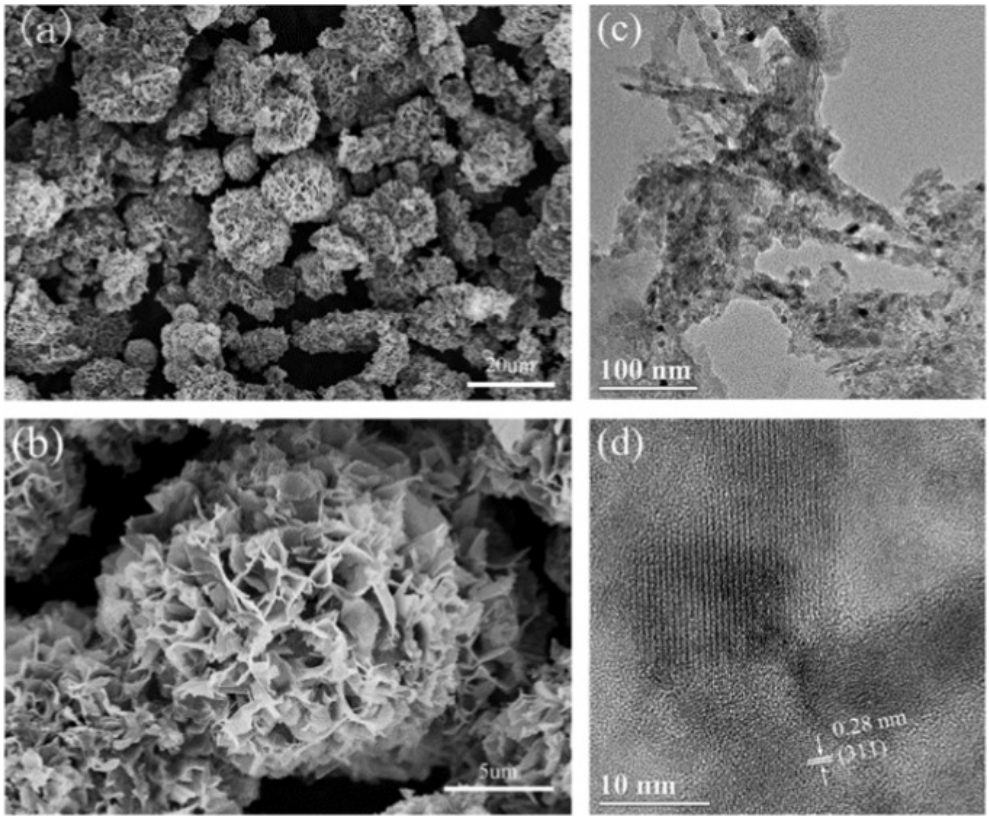
(a)
20um
(c)
100 nm
(b)
5um
(d)
0.28 nm
(311)
10 nm

Fig. 2

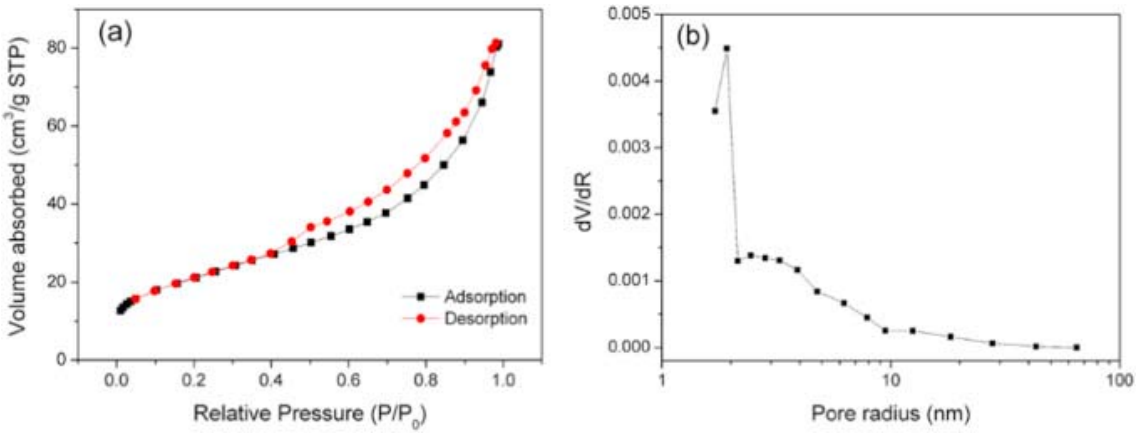
(a)
Volume absorbed (cm³/g STP)
Relative Pressure (P/P0)
Adsorption
Desorption
(b)
dV/dR
Pore radius (nm)

Fig. 3

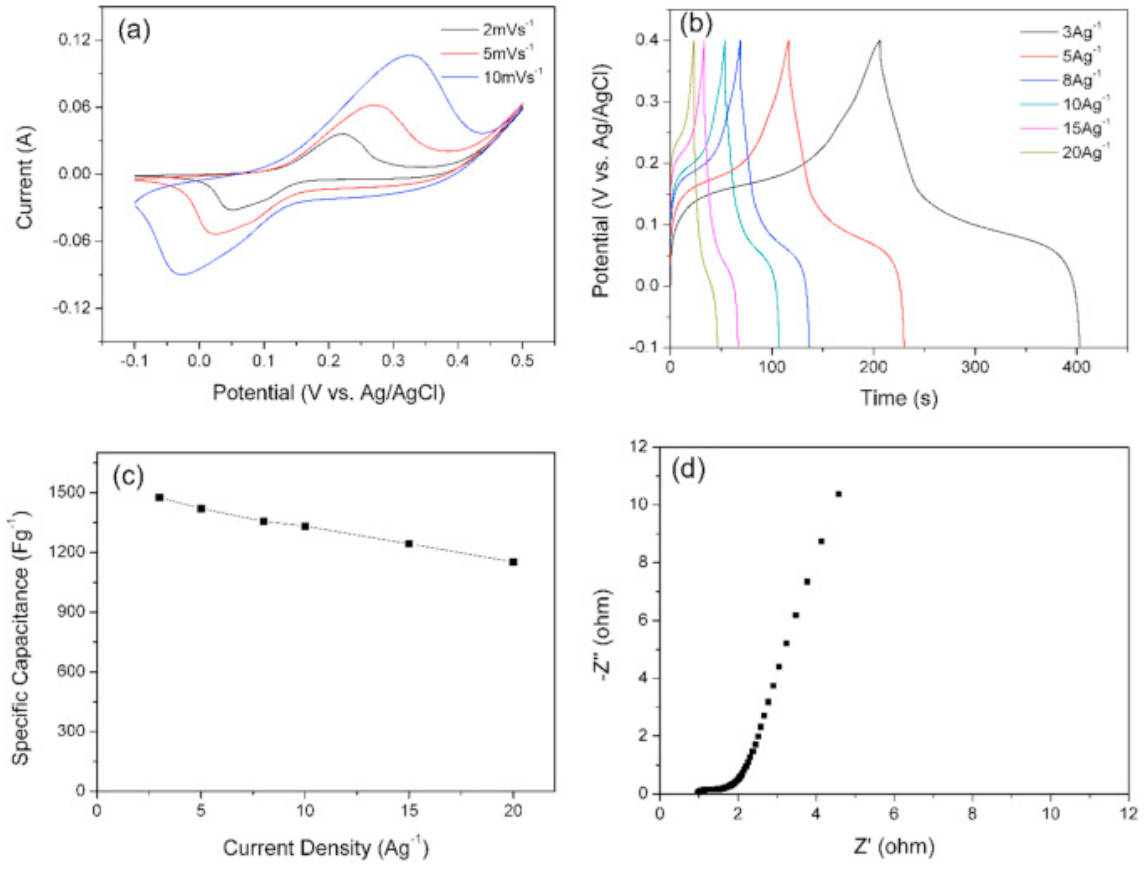
(a)
2mVs⁻¹
5mVs⁻¹
10mVs⁻¹
Current (A)
Potential (V vs. Ag/AgCl)
(b)
3Ag⁻¹
5Ag⁻¹
8Ag⁻¹
10Ag⁻¹
15Ag⁻¹
20Ag⁻¹
Potential (V vs. Ag/AgCl)
Time (s)
(c)
Specific Capacitance (Fg⁻¹)
Current Density (Ag⁻¹)
(d)
-Z'' (ohm)
Z' (ohm)

Fig. 4

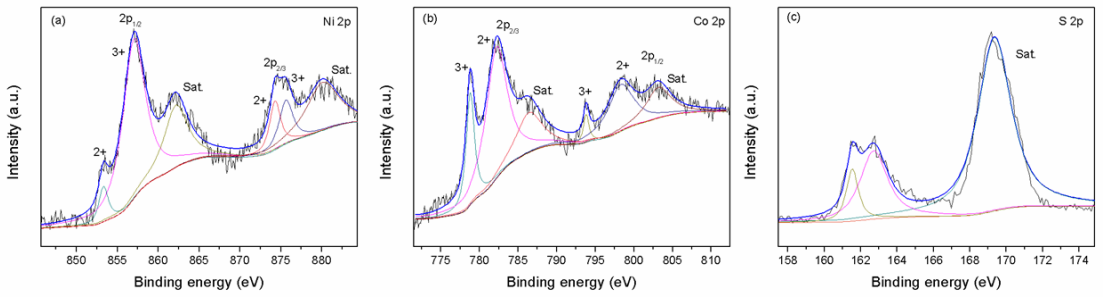
(a)
Ni 2p
2p1/2
3+
2+
Sat.
2p3/2
3+
2+
Sat.
Intensity (a.u.)
850 855 860 865 870 875 880
Binding energy (eV)
(b)
Co 2p
2p3/2
2+
3+
Sat.
3+
2+
2p1/2
Sat.
Intensity (a.u.)
775 780 785 790 795 800 805 810
Binding energy (eV)
(c)
S 2p
Sat.
Intensity (a.u.)
158 160 162 164 166 168 170 172 174
Binding energy (eV)

Fig. S1

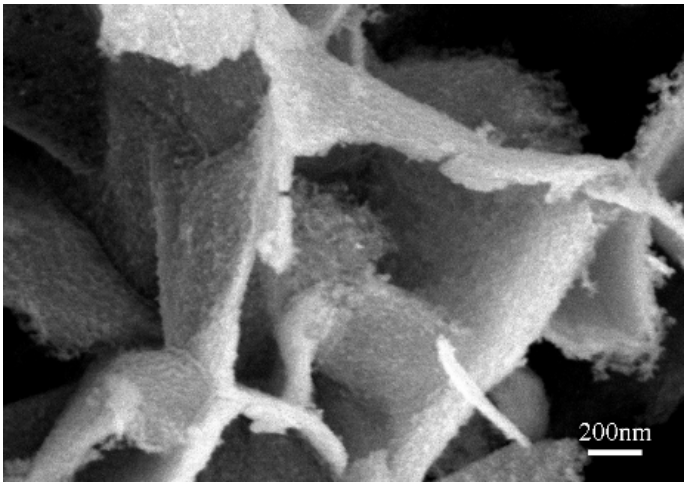
200nm

Fig. S2